3D PRINTING AND ADDITIVE MANUFACTURING
Volume 10, Number 5, 2023
Mary Ann Liebert, Inc.
DOI: 10.1089/3dp.2021.0147

ORIGINAL ARTICLE

Improving the 3D Printability of Sugar Glass to Engineer Sacrificial Vascular Templates

Brenden N. Moeun,[1] Stephanie A. Fernandez,[1] Simon Collin,[2] Gabrielle Gauvin-Rossignol,[2] Theophraste Lescot,[3–5] Marc-André Fortin,[3–5] Jean Ruel,[2] André Bégin-Drolet,[2] Richard L. Leask,[1] and Corinne A. Hoesli[1,6]

Abstract

A prominent obstacle in scaling up tissue engineering technologies for human applications is engineering an adequate supply of oxygen and nutrients throughout artificial tissues. Sugar glass has emerged as a promising 3D-printable, sacrificial material that can be used to embed perfusable networks within cell-laden matrices to improve mass transfer. To characterize and optimize a previously published sugar ink, we investigated the effects of sucrose, glucose, and dextran concentration on the glass transition temperature (T_g), printability, and stability of 3D-printed sugar glass constructs. We identified a sucrose ink formulation with a significantly higher T_g (40.0 ± 0.9°C) than the original formulation (sucrose-glucose blend, $T_g = 26.2 \pm 0.4$°C), which demonstrated a pronounced improvement in printability, resistance to bending, and final print stability, all without changing dissolution kinetics and decomposition temperature. This formulation allowed printing of 10-cm-long horizontal cantilever filaments, which can enable the printing of complex vascular segments along the x-, y-, and z-axes without the need for supporting structures. Vascular templates with a single inlet and outlet branching into nine channels were 3D printed using the improved formulation and subsequently used to generate perfusable alginate constructs. The printed lattice showed high fidelity with respect to the input geometry, although with some channel deformation after alginate casting and gelation—likely due to alginate swelling. Compared with avascular controls, no significant acute cytotoxicity was noted when casting pancreatic beta cell-laden alginate constructs around improved ink filaments, whereas a significant decrease in cell viability was observed with the original ink. The improved formulation lends more flexibility to sugar glass 3D printing by facilitating the fabrication of larger, more complex, and more stable sacrificial networks. Rigorous characterization and optimization methods for improving sacrificial inks may facilitate the fabrication of functional cellular constructs for tissue engineering, cellular biology, and other biomedical applications.

Keywords: sugar glass, glass transition temperature, printing quality, sacrificial ink, tissue engineering, vascularization

[1]Chemical Engineering, McGill University, Montreal, Canada.
[2]Mechanical Engineering, Université Laval, Québec, Canada.
[3]Axe Médecine Régénératrice, Centre de Recherche du Centre Hospitalier Universitaire de Québec (CR-CHUQ), Québec, Canada.
[4]Centre de Recherche sur les Matériaux Avancés (CERMA), Université Laval, Québec, Canada.
[5]Département de Génie des Mines, de la Métallurgie et des Matériaux, Université Laval, Québec, Canada.
[6]Biomedical Engineering, McGill University, Montreal, Canada.

Opposite page: Sugar glass made from only sucrose can be used to 3D print complex branching geometries suitable for the use in the vascularization of artificial tissue constructs via sacrificial molding. *Image Credit:* Simon Collin and Brenden N. Moeun.

This article has been updated on July 18, 2022 after first online publication of July 6, 2022 to reflect Open Access, with copyright transferring to the author(s), and a Creative Commons License CC-BY-NC added (http://creativecommons.org/licenses/by-nc/4.0/)

Introduction

TISSUE ENGINEERED CONSTRUCTS offer a promising means for replacing, restoring, and enhancing organs for regenerative medicine applications. For instance, artificial kidney, pancreas, liver, and heart constructs, among others, are being developed to treat tissue damage and disease.[1–5] Once successful, this caliber of artificial tissue could eliminate the need for donor tissue and whole organ transplants. Due to oxygen's low solubility in aqueous conditions, oxygen diffusion limitation is a major obstacle in scaling up tissue engineering technologies for human applications, which would require constructs within the cm-scale.[5,6]

To illustrate, Papas *et al.* reported that an avascular artificial pancreas (sheet geometry) for type 1 diabetes cell therapy would be expected to have a footprint on the order of 1 m^2 based on physiological oxygen tension and the upper limit of a functional cell seeding density.[7] One way to decrease the size of these devices is to build multilayer constructs where oxygen and other nutrients are transported more effectively through bulk fluid movement.

Physiologically, thick tissues are oxygenated through dense vascular networks. However, growing blood vessels within tissue-engineered constructs require prolonged growth periods during which the graft cells would have limited access to oxygen and nutrients.[8] As such, artificial vascularization has become a prominent area of interest within the tissue engineering field.[9–11] Perfusable channels can be embedded within tissue engineered constructs by casting cell-laden hydrogels around sacrificial materials, or alternatively by printing sacrificial materials directly into cell-laden matrices.[12] On solidifying the cell-laden matrix, the sacrificial material is evacuated through dissolution or liquefaction.[13–16]

By generating artificial tissues with perfusable channels, these grafts can be implanted intravascularly or between two existing blood vessels, thereby providing the device with an immediate source of oxygen and nutrients.[17,18] To limit surgical complexity, intravascular grafts generally comprise a single blood inlet and outlet. However, to optimize the oxygen transport throughout entire cm-scale devices, artificial vasculature could distribute blood flow by mimicking the branching architecture of native blood vessels. To achieve these structures in sacrificial templates, it is critical to develop the capacity to generate branching points and complex vascular networks originating from and ending at a single inlet and outlet.

Such structures require cantilever filaments as building blocks where the ability to achieve longer, more stable overhanging filaments would allow for larger constructs, complex branching, more flexibility in dimensional configurations, and circumvent the need for supporting structures during 3D printing. Due to the solid-to-liquid reversibility required of the 3D-printed templates, these constructs are typically fabricated using non-conventional 3D printing materials. For example, Pluronic® F127 hydrogel has been used to fabricate embedded vasculature by means of the material's thermo-reversible properties.

Pluronic networks are printed under warmer temperatures, at which the material behaves like a solid, and evacuated under cold temperatures, where the material behaves like a liquid.[19] Unfortunately, numerous 3D-printed hydrogels and alternative materials lack self-supporting strength, limiting their ability to form vertical or cantilever filaments.[20] Others are formulated from organic materials that can be cytotoxic or require cytotoxic conditions for sacrificial molding or demolding, making them unsuitable for cell applications.[21]

Previous studies demonstrated that sacrificial molding using sugar glass can streamline the irrigation of tissue constructs.[13,22–24] Printable sugar glass is advantageous because the material is non-toxic, inexpensive, and can be easily evacuated. The method of using 3D-printed sugar glass to generate perfusable constructs was pioneered by Miller *et al.* and was a significant step forward in engineering clinically relevant artificial vasculature.[25] This initial platform was limited by an incapacity to generate cantilever structures and print directly in the z-axis. This printing strategy also subjects filaments to pulling forces during extrusion, resulting in a tapered cross-sectional area.

Recently, our group engineered a novel printing platform permitting the fabrication of vertical and self-supporting filaments.[14] The printing strategy uses a 2-zone temperature control system and cooling air jets for the rapid vitrification of molten sugar glass. This novel printing platform has an xyz-axis printing capacity and can either maintain or vary the cross-sectional area of printed filaments. The system is capable of printing objects such as the Stanford bunny, branched networks, and molds that can be cast with different materials.[26]

The sugar glass ink used in the earlier mentioned work utilized the same base composition as that of Miller *et al.* but was heated to a higher temperature, allowing for increased caramelization.[14] Although this ink was suitable for printing small constructs and simple geometries, longer and more complex networks tended to deform and collapse during printing and at ambient conditions. We hypothesized that the glass transition temperature (T_g) of the ink was too close to room temperature range and led to poor printability and difficulty in post-print handling.

Notable examples of alternative sugar formulations in the field include sucrose-glucose-dextran mixtures[25,27] and sucrose-glucose blends,[14,28] which demonstrated promising results in their use in culturing cell lines such as 10T1/2 cells and primary cells (e.g., human umbilical vein endothelial cells). Work from the Miller and Atluri groups showed that these materials could be used to generate perfusable cell encapsulation constructs with hydrogels requiring various crosslinking mechanisms (e.g., alginate, agarose, and polyethylene glycol [PEG]) and demonstrated blood flow and patency in polydimethylsiloxane (PDMS) constructs implanted into rats.[25,29]

Fibrin and PEG constructs were also used to demonstrate the endothelialization of channels with HUVECs and improved cell function in primary rat hepatocytes when compared with non-perfusable constructs, respectively.[25] Moreover, Farzin *et al.* developed a sucrose-glucose-dextran blend supplemented with sodium citrate to 3D print dissolvable stents, which facilitated vascular anastomosis, hemocompatibility, and antithrombogenic properties when implanted into porcine femoral arteries *ex vivo*.[27] The use of molten sugar alcohols has also shown potential in the area of artificial vascularization due to the materials' optical transparency that facilitates the use of encapsulation materials that gel via photopolymerization.

A Maltitol ink has been used to generate perfusable PDMS constructs for culturing a human ovarian cancer cell line (SKOV3 cells),[30] and 3D-printed isomalt has been used to generate cantilever constructs.[31,32] Much of the current sugar glass 3D printing work has focused on generating 2D networks, which still limits the scale of tissue constructs. Of the

groups who printed sugar glass constructs in xyz, only short self-supporting channels were demonstrated (~5 mm), small-scale branched networks were achieved, preparation under vacuum and specific storage conditions were required, and the capacity to generate perfusable branched networks in cell-laden hydrogels was not shown.

Although several promising sugar formulations have been proposed as described earlier, there has been inconsistent characterization of these materials between groups to assess properties relevant to tissue engineering. Selection of appropriate sugar formulations may vary depending on specific aspects of artificial tissue construction, such as hydrogel properties, cell types, and construct geometry. It is therefore important to establish a methodological toolkit for rigorous characterization and optimization of different sugar inks with the aim of increasing the general relevance of sugar printing in the field of tissue engineering.

As a starting point, this work describes a set of methods to characterize and optimize the glucose-sucrose ink our group previously utilized with our custom printer head.[14] To accomplish this, modifications in the ink formulation were made to increase the T_g. Thermophysical properties, mechanical properties, and printability were evaluated to identify a formulation capable of reliably producing complex printed networks and self-supporting structures. Here, printability is characterized by the capacity to print human-scale vascular templates. As such, we focus on the potential of inks to print cm-scale, mechanically stable, and multi-branched networks representing arteries or veins without the use of supporting materials. This work provides a basis for elaborating a comprehensive set of design considerations and setting up future studies to evaluate the performance of candidate sacrificial materials for artificial vascularization strategies.

Methods

Sugar glass preparation

Sugars (D-sucrose and glucose; Fisher) amounting to a combined 78.0 g were added to 50 mL of reverse osmosis (RO) water within a 250-mL beaker and heated for 15–18 min until the solution reached 90°C on a hotplate (Scilogex MS7-H550-Pro). This intermediate heating step was used to visually ensure that all sugar crystals were dissolved before the final heating stage to prevent sucrose recrystallization. The solution was then heated for ~30 min until it reached 175°C. The solution was removed from the heat immediately on reaching 175°C and, when applicable, 0.79 g of dextran (Mr ~100,000; Sigma) was stirred in.

During the heating process, the hotplate's built-in feedback temperature control system was implemented. Throughout the entire process, the solution was stirred without being covered at 400 rpm using a 1″ magnetic stir bar. Samples that were 3D printed or cast were stored and transported in desiccated and evacuated chambers at ambient temperature and/or maintained at 4°C until use.

Thermophysical characterization

Differential scanning calorimetry was conducted on 5–10 mg samples of sugar glass in hermetically sealed pans using heat/cool/heat cycling between −15°C and 70°C with a heating and cooling rate of 3°C/min under air (TA Instruments, Q2000). T_g were determined from the second heating cycle using TA Universal Analysis software. Thermogravimetric analysis was conducted from ambient conditions up to 500°C using a heating rate of 10°C/min under air (TA Instruments, Q500). Decomposition temperatures (T_ds) were determined using TA Universal Analysis software and were defined at the onset of mass loss.

Temperature-dependent viscosity curves were generated using a dynamic parallel plate (25-mm diameter) configured rheometer (Anton Paar MCR 302 with CTD 450 attachment) and a constant angular frequency (0.5 Hz). A 1-mm measuring gap and a temperature ramp of 3°C/min were implemented between 130°C and 40°C under air. As described by Jiang *et al.*, the degree of caramelization was evaluated using an ultraviolet-visible spectrometer (Thermo Scientific, Evolution 220).[33] Sugar glass formulation samples were diluted in RO water to concentrations, yielding absorbance measurements between 0.1 and 1 and pure RO water was used as a reference.

Absorbance at 420 nm of solutions with the same concentrations was used to characterize the yellow-brown color of the materials, whereas absorbance at 284 nm was used to quantify the concentration of 5-(hydroxymethyl)furfural (HMF). Serial dilutions of a stock HMF (98%; Thermo Scientific) solution were used to generate a calibration curve.

Dissolution kinetics

Samples cast for studying dissolution kinetics were prepared using hemispherical silicone wells (2.5 cm in diameter). Once the sugar preparation procedure was completed, 3 mL of molten sugar glass ink was poured into each of the wells using a syringe. Samples were then cooled and stored in a desiccator at ambient temperature until use. Hemispherical samples of sugar glass were submerged in 40 mL of 4-(2-hydroxyethyl)-1-piperazineethanesulfonic acid-buffered saline solution and stirred in an orbital shaker at 170 rpm. HEPES-buffered saline solution was prepared with 170 mM sodium chloride (Fisher) and 10 mM HEPES (Fisher) followed by the addition of 2 M sodium hydroxide until the solution reached pH 7.4.

Sample mass was measured at 3-min intervals until complete dissolution, evaluated by visual inspection. To compare dissolution kinetics among formulations, rate constants were evaluated by fitting the data to a first-order decay function using GraphPad Prism 5.01 software.

Sugar glass 3D printing

Immediately after preparation, molten carbohydrate inks were loaded into 20-mL glass syringes (Fortuna Brand), which were then inserted into a modified Airwolf AW3D XL printer. This printer was equipped with the printer head previously developed by Bégin-Drolet *et al.*, and two cooling air jets were placed on opposite sides of the nozzle outlet.[14] Printer temperature was selected to encourage optimal printability, minimal additional caramelization, and rapid solidification of the original material (80–99°C depending on the formulation). Using temperature control, the viscosities of alternative formulations were set to equal the viscosity of the original material within the nozzle of the printer head. Custom G-codes were written to test the longest cantilever filament length and print stability of each ink.

Flexural strength testing

Sugar glass filaments were 3D printed at Université Laval (Quebec City, Quebec, Canada), vacuum sealed with

desiccant, stored at 4°C, and shipped to the mechanical testing laboratory at McGill University (Montreal, Quebec, Canada; ~250 km and 3–5 h transport duration from pick-up to drop-off). Samples were tested within 24 h of receipt according to ASTM C1684. All tested filaments were analyzed as two distinct groups, sorted by shipping date. Flexural strength was measured using a universal strength testing machine (Shimadzu EZ Test, 500N Capacity).

Cylindrical samples with a diameter of 2 mm and a support span of 30 mm were tested. A strain rate of 5 mm/min was used. Formulations were prepared in triplicate batches, with two to four printed samples being tested for each sugar glass variation.

Print quality and stability of constructs

Stability of printed constructs in ambient conditions. Immediately after printing, samples were transferred to an automated photo booth and left in ambient conditions. Digital photos were acquired every hour. The minimum filament height (i.e., distance between the lowest point of the filament and the base plate) for each picture was then determined using a custom MATLAB® code. Data were standardized by converting minimum heights into maximum absolute vertical deflections relative to initial height.

Cantilever filament length. Maximum cantilever filament length was determined for different sugar glass formulations by printing overhanging filaments of various lengths. All filaments were 1 mm in diameter and were supported at one end by two parallel walls measuring 10 mm tall and spaced 10 mm apart (i.e., simply supported filaments). The double wall was incorporated to minimize pulling forces while printing and to avoid a full moment connection cantilever beam. There were no supports at the other end of the filaments. Printing was conducted at ambient conditions (24–25°C and 32–44% relative humidity). The extrusion speed and cooling jet settings were identical between all prints. Digital images were captured immediately after the constructs were printed; however, prints took ~30 min to complete.

Suspended filament lengths of 40, 60, 80, and 100 mm, measured from the inner supporting wall, were printed sequentially on the same construct (Fig. 5a, b). If a notable vertical deflection was observed for a specific length, the previous length was taken as the maximum printable length.

Print quality of complex vessel network templates. Print quality was qualitatively assessed by printing a complex network of filaments (Fig. 5c–e). The construct had 18 branched filaments and was 83 mm long. Printing was conducted at ambient conditions (24–27°C and 31–44% relative humidity). The extrusion speed and cooling jet settings were identical between all prints. Digital images were captured immediately after printing, and results from each recipe were compared. Finally, filaments 80 mm in length and supported at both ends (Fig. 6b, c) were printed and stored at ambient conditions (22–26°C and 20–23% relative humidity) for 7 days to test the storage stability of the ink formulations.

Geometrical conformity studies by micro-computed tomography imaging. Print quality was further assessed by comparing the final dimensions of 3D-printed constructs, measured by X-ray micro-computed tomography (μCT), with the initial computer-aided design (CAD) plans. First, a 3D model of a nine-branch construct (eight 1-mm channels and one central 1.6-mm channel) was created using PTC Creo Parametric software (version 3.0). This file was used to 3D print a sugar glass network, which was then imaged using a μCT system (eXplore Locus 80; GE Healthcare). Scans were performed at 40 kV (current: 100 mA).

The detector exposure time was 100 ms and detector binning was 4×4 for a voxel resolution of 89 μm with three frames averaging. Image reconstructions were performed with the Parallax Innovations Reconstruction tool from Parallax Innovations (Ilderton, Canada). Image visualization and segmentation were performed using MicroView from Parallax Innovations (Version: 2.5.0, Ilderton, Canada). The 3D model developed for the segmentation step was used as the numeric reference for the 3D-printed sugar sample. The 3D-printed reference and original CAD model were then numerically superimposed to qualitatively assess the print fidelity and geometrical conformity. Numerical deviations from the CAD model were calculated using the ''Distance from Reference Mesh'' function from MeshLab software, version 2016.12. A heat map was generated using these deviations superimposed upon the 3D sugar model.

Fabrication of perfusable alginate constructs. Branched sugar glass networks were used to generate perfusable alginate constructs to demonstrate patency and the capacity to generate hollow channels of varying dimensions. For these experiments, sugar constructs containing calcium chloride were 3D printed. To generate these constructs, sugar formulations were first prepared as described earlier and then mixed with a small volume of a secondary sugar formulation containing calcium chloride. This secondary formulation was prepared by combining 5.0 g of sucrose (Fisher), 1.2 g of glucose (Fisher), and 0.4 g of calcium chloride (Sigma) in 40 mL of demineralized water.

This sugar mixture was stirred at 200 rpm and heated on a hotplate (Scilogex MS7-H550-Pro) until it reached 140°C and then mixed with the primary sugar glass formulation. The combined sugar glass ink was then loaded into a preheated syringe and used to 3D print 9-branch vascular templates. These constructs were also dip-coated in an ethanol bath containing 210 mM calcium chloride and left to dry. The coated networks were then loaded within a custom-built cylindrical polycarbonate mold. The void space surrounding the sugar network was filled with an HEPES-buffered alginate solution of concentrations 2.5% w/v alginate (Manugel GHB, FMC BioPolymer), 30 mM calcium carbonate ($CaCO_3$; Avantor), and 60 mM glucono-δ-lactone (GDL; Sigma).

The alginate solution was left to gel at room temperature for 20–30 min. The embedded sugar construct was evacuated using an oscillating peristaltic flow (3 mL/min) from a peristaltic pump, and the irrigated construct was perfused with water containing red food coloring. For imaging, perfusable constructs were deposited into a bath of demineralized water for 24 h. The alginate constructs were then imaged by μCT, and characteristic slices were selected to show areas of interest (Fig. 6f).

Cell culture and cell viability

Mouse insulinoma 6 (MIN6), a pancreatic beta cell line, was generously provided by Dr. Jun-ichi Miyazaki, Osaka University. MIN6 cells were cultured on adherent, tissue culture-treated polystyrene flasks at 37°C and 5% CO_2.

Complete culture medium consisted of Dulbecco's modified Eagle's medium supplemented with 10% fetal bovine serum (HyClone™; Thermo Fisher Scientific), 100 U/mL penicillin/streptomycin (Gibco; Thermo Fisher Scientific), 2 mM L-glutamine (Gibco; Thermo Fisher Scientific), and 50 μM β-mercaptoethanol (Fisher). The medium was changed every 48 h until cells reached 90% confluency, after which cells were passaged using TrypLE Express Enzyme (Gibco; Thermo Fisher Scientific). MIN6 of passage 30 and below with 90% viability or above (measured via trypan blue) were used in the following experiments.

A suspension of MIN6 cells in complete medium making up 10% v/v of the final solution volume was gently stirred into an alginate mixture with $CaCO_3$ and GDL, as described earlier (2.5% w/v final concentration). The final viable cell seeding density was 40×10^6 cells/mL. The cell-laden alginate solution was then cast around sugar filaments held in place with custom PDMS connectors within a 48-well plate (Sarstedt, Germany). The sugar glass filaments were 2 mm in diameter and made by casting the respective molten formulations into PDMS molds. The alginate was left to gel for 30 min in a standard cell culture incubator, after which the gels were removed from the wells and washed with complete medium for 30 min at 37°C.

The constructs were then manually sliced using a razor blade and stained in an HEPES-buffered saline solution containing 10% v/v complete medium, 4.0 μM Hoechst stain (Life Technologies), 2.0 μM calcein AM, and 2.0 μM ethidium homodimer-1 (Live/Dead® Viability/Cytotoxicity kit; Invitrogen) for 30 min. Entire slices were imaged using an Olympus IX81 fluorescence microscope (Olympus, Japan) equipped with a pre-programmable Prior® stage (Prior Scientific, Inc.). Individual microscope images were stitched together using ImageJ software to visualize the complete cross-sectional slices of the constructs. Cell viability around resulting channels was quantified by counting maxima using ImageJ software to analyze fluorescence intensity.

Statistical analysis

T_g, T_d, flexural strength, maximum deflection, and cell viability data are represented as the mean ± the standard error of the mean from triplicate experiments. Statistical significance was evaluated using JMP software through one-way analysis of variance (ANOVA) and Tukey significant difference *post hoc* testing with a threshold of $p < 0.05$ unless otherwise mentioned. Practical equivalency in viability was determined using two one-sided tests with a threshold of $p < 0.05$ for differences of >5%. Rheological data were fit to the Williams-Landel-Ferry equation with a reference temperature of $T_g + 43$ K.[34]

The models were plotted with a 95% confidence interval on the collected data using JMP software. Dissolution kinetics data were collected in triplicate and fit to a first-order kinetics model using JMP software. Statistical significance was evaluated by comparing the fitted rate constants with $p < 0.05$.

The effects of the formulation and shipping dates on the flexural modulus were assessed using the 2^2 factorial design shown in Eq. (1).

$$E_f = \beta_o + \beta_1 x_1 + \beta_2 x_2 + \beta_{1,2} x_1 x_2 \quad (1)$$

where E_f is the flexural modulus, β_o is the intercept regression coefficient, β_1 is the regression coefficient for the formulation, β_2 is the regression coefficient for the shipping date on E_f, and $\beta_{1,2}$ is the regression coefficient for the interaction of the formulation and shipping date.

The variable x_1 is a categorical variable representing the formulation, with a value of 1 attributed to one formulation and −1 to the other. The variable x_2 is a categorical variable representing the shipment date, with a value of 1 attributed to one shipping date and −1 to the other. The linear model was constructed and analyzed using JMP software.

Results

Desired properties for sugar glass inks

Table 1 summarizes the desired properties of a sugar glass 3D printing ink and printing system in the context of generating vascular templates for tissue engineering. The presented properties and rationale were used to direct the characterization strategy for the sugar glass formulations in this work. They may also serve as guidelines for future optimizations of sacrificial inks for artificial vascularization. Here, the characterization of inks was started by increasing the T_g of our original ink formulation (original).

Materials with T_g exceeding room temperature are generally characterized by greater stability, strength, and print quality, and this would result in a more reliable 3D printing platform.[35] Models for the T_g of amorphous blends, such as the Gordon-Taylor equation and the Couchman-Karasz model, propose a proportional relationship between the T_g and mass fractions of the base materials with the T_g of the blended material.[36,37]

Thermophysical properties

Materials with T_g exceeding ambient conditions are expected to better maintain their rigidity and stability throughout printing and storage, leading to improvements in print quality and fidelity. To test this hypothesis, we measured the T_g of different sugar glasses prepared from varying base materials. The original ink formulation (original) developed for the custom 3D printer was prepared using a 2:1 sucrose-to-glucose mass ratio.[14] As a point of comparison, the T_g values of sucrose and glucose were considered to be 60°C and 23°C, respectively, as reported in literature.[38]

Figure 1a demonstrates that sugar glass variations prepared entirely of sucrose (S100) or with a 4:1 ratio of sucrose to glucose (S80) were found to significantly increase the T_g when compared with the original formulation.

Although the T_g of dextran is dependent on molecular weight, water content, and branching, an approximation of 180°C can be made for the dextran used in these experiments based on the correlation published by Icoz *et al.*[39] The addition of dextran was, thus, expected to further increase the T_g of the resulting sugar glass. Formulations with 1% added dextran, denoted as S100D1 and S80D1, demonstrated significantly higher T_g values when compared with the formulations without dextran. Sucrose recrystallization was not observed when preparing any of these formulations.

The T_d represents the point at which the onset of material degradation occurs, ultimately altering the chemical composition of the material and potentially leading to different physical behavior. Values of T_d were measured to establish an upper limit for the printing process and other thermophysical characterization studies. The S80 and S80D1

Table 1. Desired Properties and Characterization Considerations for Engineering Sacrificial Sugar Glass Inks for Artificial Tissue Vascularization

Category	*Desired properties*	*Description*
Printing	T_g greater than ambient conditions	Promotes rapid solidification and integrity of printed structures
	T_d greater than extrusion temperature	Mechanical and thermophysical properties remain stable at an extrusion temperature acceptable for 3D printing (i.e., resulting in a suitable viscosity, $\sim$500 Pa·s)
	No ink crystallization	Crystallization during printing can cause nozzle blockages and geometrical defects
	Capacity for constructs to be printed without supports	Streamlines overall process by simplifying 3D printing needs and post-print processing
	Printed filaments withstand forces associated with printing	Permits the use of cooling air jets to promote rapid solidification and maintains construct integrity amid pulling forces exerted by printing nozzle
	High level of print fidelity in constructs	Sacrificial ink and printing system accurately reproduce geometries and dimensions from CAD files
	Printed filaments have a smooth finish and result in smooth channel walls	Roughness can cause disruptions in perfusate flow, increased flow pressure drops, and thrombogenesis.
Sacrificial molding	Negligible cytotoxicity	Cells remain viable and functional after exposure to the sacrificial ink (both while solid and during ink evacuation)
	Printed networks withstand forces associated with artificial tissue construction	Maintains geometric integrity during handling and casting cell-laden materials
	Simple and easy evacuation of the sacrificial material	Facilitates overall tissue engineering process and reduces time between tissue construction and perfusion (i.e., decreases risk of nutrient and/or oxygen exhaustion)
	Perfusable channels in tissue constructs maintain geometry of vascular templates	Perfusion channels can be generated in a predictable and controlled manner
Storage	Prints stable at ambient conditions	Eases storage requirements, permits the usage of prints generated days in advance, facilitates the shipment of printed constructs, and prints can be stored without supports

CAD, computer-aided design; T_d, decomposition temperature; T_g, glass transition temperature.

formulations were omitted from further testing and analysis due to their lower T_g when compared with S100 and S100D1. The latter two formulations were tested for T_d alongside the original ink. As shown in Figure 1b, no significant differences in T_d were identified. Maximum temperatures for differential scanning calorimetry, rheometry, and 3D printing were all set well below these values.

To conserve the printing viscosity between the different ink formulations, the printer temperature settings required adjustment. The 3D printer was originally designed and optimized according to the viscosity of the original ink within the nozzle of the printer head.[14] In this initial work, the nozzle temperature was set to 80°C, which corresponds to a material viscosity of 529 ± 2 Pa·s. To determine the appropriate printing temperature for the new ink formulations, the effect of temperature on material viscosity was measured between T_g and T_d. Figure 1c and d shows the Williams-Landel-Ferry model that was fit onto the raw temperature-viscosity data of the original, S100, and S100D1 formulations.

Notably, S100 and S100D1 are more viscous materials within the prescribed temperature range and therefore require higher temperature settings within the printer head to maintain a comparable rheological profile during printing. The nozzle temperature for S100 was set to 95°C, and the nozzle temperature for S100D1 was set to 99°C.

The degree of caramelization was also characterized, as this type of heating process is understood to affect the T_g of sugar glass materials.[33] To do this, the concentration of HMF was measured and the yellowish-brown color of the original and S100 materials was evaluated using spectroscopy. As shown in Figure 1e, the concentration of HMF in the original formulation was significantly higher when compared with the S100 ink. Similarly, a significantly greater absorbance at 420 nm was measured in the original ink, which indicates a deeper yellowish-brown pigment (Fig. 1f). Both findings suggest that the degree of caramelization is greater in the original formulation when compared with the S100.

Sugar glass dissolution kinetics

Once a 3D network is printed from sugar glass, the network is embedded within a cell-laden material and dissolved, leaving behind hollow, perfusable channels. To conserve the quick and efficient evacuation demonstrated by the original ink, the alternative formulations should possess similar dissolution kinetics. The dissolution of sugar glass variations in HEPES buffer was monitored on a mass basis and the data were fitted to a first-order rate kinetics model, shown in Figure 2. Statistical differences between fitted rate constants of the original, S100, and S100D1 formulations were not observed.

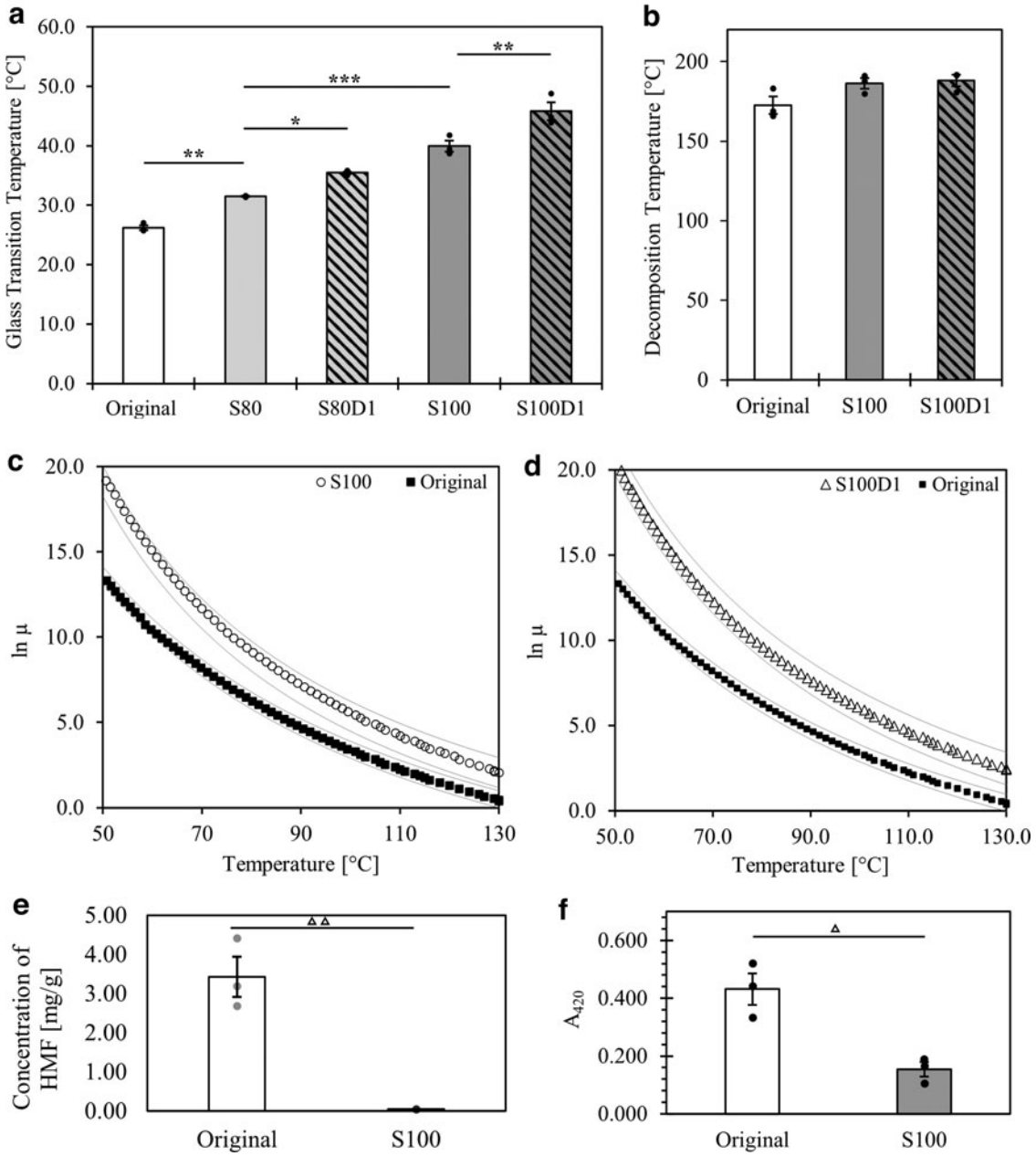

FIG. 1. Thermophysical data of original material and alternative formulations. **(a)** T_g of sugar glass formulations. $^{*}p < 0.05$, $^{**}p < 0.01$, and $^{***}p \leq 0.0005$ by one-way ANOVA and Tukey HSD *post hoc* test. The original material used by Bégin-Drolet *et al.* (original), 4:1 sucrose-to-glucose mass ratio (S80), 4:1 sucrose-to-glucose mass ratio with 1% w/w added dextran (S80D1), entirely sucrose (S100), and entirely sucrose with 1% w/w added dextran (S100D1). **(b)** T_ds of sugar glass formulations. No statistical significance was found between the means through a one-way ANOVA and Tukey HSD *post hoc* test. **(c, d)** Representative temperature-dependent viscosity data of sugar glass formulations. Viscosity is denoted as μ and is reported in MPa·s. Area enclosed by *solid gray lines* represents a 95% prediction confidence interval of a Williams-Landel-Ferry model fitted to the data.[25,28] Samples shown are the original (*squares*, $R^2 = 0.997$), S100 (*circles*, $R^2 = 0.995$), and S100D1 (*triangles*, $R^2 = 0.994$) formulations. **(e, f)** Measure of HMF using 284-nm absorbance and *yellow-brown color* using 420-nm absorbance of the original and S100 formulations, respectively. $^{\Delta\Delta}p < 0.005$ and $^{\Delta}p < 0.05$ by *t*-test and Tukey HSD *post hoc* test. ANOVA, analysis of variance; HMF, 5-(hydroxymethyl)furfural; HSD, honestly significant difference; T_d, decomposition temperature; T_g, glass transition temperature.

Mechanical strength testing

Mechanical stability of 3D-printed structures is critical throughout the printing process, as well as during transport, storage, and manipulation of the constructs. The flexural strength and bending resistance of 3D-printed sugar glass formulations were evaluated using 3-point bending tests. Generally, the sugar glasses predominantly demonstrated brittle mechanical characteristics, failing shortly after linear stress-strain behavior (data not shown). For simplicity, comparative printing analyses were only conducted between the original and all-sucrose inks (S100 and S100D1). Despite

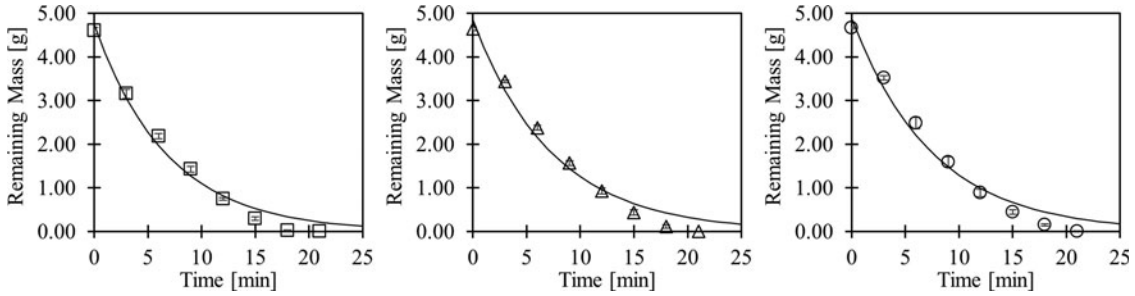

FIG. 2. Dissolution comparison of sugar glass variations in HEPES buffered saline solution. Samples shown are the original (*squares*, $R^2 = 0.979$), S100 (*triangles*, $R^2 = 0.979$), and S100D1 (*circles*, $R^2 = 0.974$) formulations. Data were fitted to a first-order kinetics model, and no significant differences between rate constants were calculated through the extra sum-of-squares *F*-test. HEPES, 4-(2-hydroxyethyl)-1-piperazineethanesulfonic acid.

an increase in T_g (Fig. 1a), the formulation supplemented with dextran (S100D1) introduced extrusion difficulties such as nozzle blockages caused by undissolved particles.

Further, the higher temperature needed to print this formulation promoted continuous caramelization of the ink during prolonged printing experiments, such as those required for larger lattices (Fig. 5). These printing challenges caused inconsistency between prints and the S100D1 formulation was, therefore, omitted from subsequent testing for print quality and stability.

The flexural strengths of filaments printed using the original and S100 inks were not statistically different ($p = 0.46$). The flexural strength of the original ink was measured to be 80 ± 10 MPa, whereas the S100 ink withstood a maximum flexural stress of 68 ± 8 MPa. The flexural moduli of the formulations were measured to evaluate bending resistance. The S100 ink demonstrated a statistically superior resistance to bending when compared with the original ink, as shown in Figure 3.

A factorial analysis was used to evaluate the effects of variables that were suspected to impact the flexural moduli of the sugar glasses. The flexural modulus was modelled as a simple linear regression dependent on the formulation (variable 1), the shipment/preparation date (variable 2), and their interaction as nominal effects. The intercept (β_o) and the regression coefficients for the formulation (β_1), shipment (β_2), and their interaction (β_{12}) were calculated to be 8.6, 1.8, 0.7, and –0.4 GPa, respectively, each with a standard error of ±0.2 GPa.

Statistically significant effects of the formulation ($p < 0.0005$) and the shipment ($p < 0.01$) were observed, whereas no significance was calculated from the interaction effects ($p = 0.1343$). Positive regression coefficients were attributed to the S100 formulation and the second shipment date (B). Negative values described the original formulation and the first shipment date (A). A summary of the regression coefficients of the model is shown in Eq. (2), where values are reported in GPa.

$$E_f = 8.6 + \begin{cases} \text{S100} \rightarrow & 1.8 \\ \text{Original} \rightarrow & -1.8 \end{cases} + \begin{cases} \text{Shipment A} \rightarrow & -0.7 \\ \text{Shipment B} \rightarrow & 0.7 \end{cases} + \begin{cases} \text{Original} \rightarrow & \begin{cases} \text{Shipment A} \rightarrow & -0.4 \\ \text{Shipment B} \rightarrow & 0.4 \end{cases} \\ \text{S100} \rightarrow & \begin{cases} \text{Shipment A} \rightarrow & 0.4 \\ \text{Shipment B} \rightarrow & -0.4 \end{cases} \end{cases} \quad (2)$$

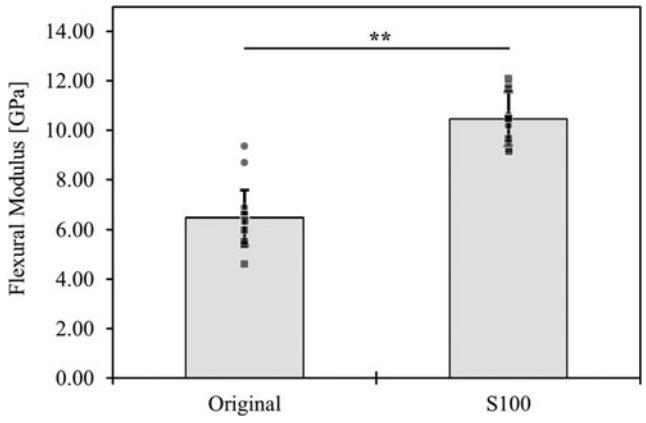

FIG. 3. Flexural modulus of the 3D-printed original and sucrose-only (S100) filaments. $^{**}p < 0.01$ by *t*-test and Tukey HSD *post hoc* test. Samples from shipment A and shipment B are shown as *squares* and *circles*, respectively.

Stability of printed constructs in ambient conditions

A capacity to maintain the geometric integrity of sacrificial vascular molds at ambient conditions would facilitate the long-term storage, transportation, and accessibility of this technology. To assess this, the depression of suspended filaments printed using the original and S100 inks was tracked over a period of 16 days (Fig. 4).

Clear differences between the two formulations are observed in Figure 4b and c. Although the original filaments reached the base of the plate after roughly 100 h, the depression in the S100 filaments was undetectable. The S100 filaments were stable for up to 16 days, after which no further data were collected. Figure 4 shows the time-lapsed deformation quantification and overlain images of filaments immediately and 7 days after printing. Time lapse videos from these studies are shown in the supplementary materials for this article as Supplementary Video S1 for the original ink and Supplementary Video S2 for the S100 ink.

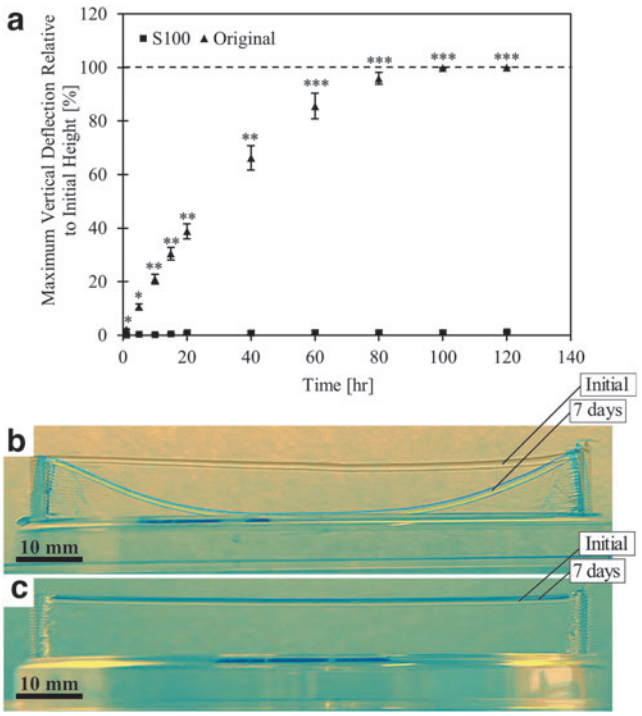

FIG. 4. Stability analysis of original and sucrose-only (S100) inks. **(a)** Print stability test samples fabricated using the original and S100 recipes and stored at ambient conditions (22–26°C, 20–23% relative humidity) for 7 days. Results are only shown up to 120 h, as no changes were observed beyond this point. Maximum vertical deviations relative to the initial height are presented ($n = 3$ for each condition). $*p < 0.005$, $**p < 0.001$, $***p < 0.0001$ by *t*-test and Tukey HSD *post hoc* test. **(b, c)** Test samples fabricated using the original and S100 formulations, respectively. Shown are *overlain* pictures of the samples immediately and 7 days after printing at ambient conditions (22–26°C, 20–23% relative humidity). The nozzle of the printer head was set to 80°C for the prints in the original ink and to 95°C for the prints in the S100 ink.

Print quality

Unlike conventional additive manufacturing, printing vascular templates is not performed layer by layer. Instead, it relies on the capacity to produce networks and cantilever structures. Using the original and S100 sugar glass inks, the maximum cantilever filament length was characterized to gauge the suitability for 3D printing cm-scale vascular templates. Similar to the mechanical strength testing, formulations that included dextran were omitted since they presented difficulties with nozzle blockages, in controlling the level of caramelization, and in achieving consistency between prints.

Figure 5a and b illustrate an improvement in the production of self-supported filaments, and Figure 5c–f show the capacity to generate more complex vascular molds using the S100 ink when compared with the original ink. Minimal deformation is observed for 100-mm filaments using the S100 ink, whereas notable collapse is observed in filaments exceeding 40 mm in length using the original ink.

Larger and more complex vascular templates would accommodate artificial tissue designs with high cell densities and cm-scale dimensions. To evaluate the flexibility of the inks in this regard, complex constructs were printed and visually analyzed. For both formulations, areas with highest deviation from input designs were observed at branching points and junctions—in particular, at points where extrusion was stopped and re-initiated to deposit additional filaments. Although constructs printed with the original ink demonstrated significant deformations, those printed using the S100 ink had rigid, straight, and cleaner filaments (Fig. 5c–f).

To further evaluate the print fidelity of branched vascular templates using the S100 formulation, the geometries of 3D-printed constructs were directly compared with their corresponding CAD models using images acquired by X-ray μCT. Figure 6a shows the CAD model used to generate a vascular network with nine branches, and Figure 6b depicts a 3D reconstruction of the printed network obtained via μCT. These images are superimposed in Figure 6c to qualitatively demonstrate the achieved print fidelity. Overall, the 3D geometry was well preserved in the print with minor deviations in the exact spatial location of the branches and in the final diameter of the printed filaments.

In a few cases, the position of the branches appears to be slightly shifted and the diameters of some printed filaments are smaller when compared with the CAD model (Supplementary Fig. S1a–f). The deviations between the 3D print and the CAD model were quantified and mapped in Figure 6d. Overall, the 3D-printed construct exhibited mostly minor and intermediate deviations. The voxels exhibiting the few major deviations were located near the entry and exit points of the vascular template. Of note, the same print and analysis with the original ink was not possible due to the continuous deformation in the branched filaments over time, particularly at the entryways.

This limitation with the original formulation was especially highlighted in longer constructs that spanned beyond 4 cm (Fig. 5c). This analysis further emphasizes the high level of print fidelity achieved with the S100 ink.

Generating perfusable constructs

The effective use of sacrificial vascular templates in tissue-engineered constructs relies on the capacity to generate perfusable networks that maintain the 3D geometry of the template. As a proof of concept, 9-branch constructs printed using the S100 formulation were used to create perfusable channels within alginate (Supplementary Fig. S2). Figure 6e shows an alginate construct that was perfused with red food coloring, and Figure 6f shows representative cross-sections of the construct. The channels generated not only appear to moderately conserve the diameters of filaments from the starting vascular template (i.e., 1 mm for the eight branched filaments, 1.5 mm for the central filament, and 4.5 mm for the inlet and outlet) but also exhibit some irregularity at the channel walls.

The average diameters of the branched, central, and inlet/outlet channels were measured to be 1.08 ± 0.02 mm, 1.47 ± 0.03 mm, and 4.43 ± 0.08 mm, respectively. Overall, the generated constructs show that the S100 ink formulation has the capacity to generate perfusable branched networks with channels of controlled diameters (1–4.5 mm) within cm-scale alginate devices.

Acute cytotoxicity toward pancreatic beta cells in alginate casts

In generating tissue-engineered constructs, it is imperative that the sacrificial template is not toxic to the surrounding

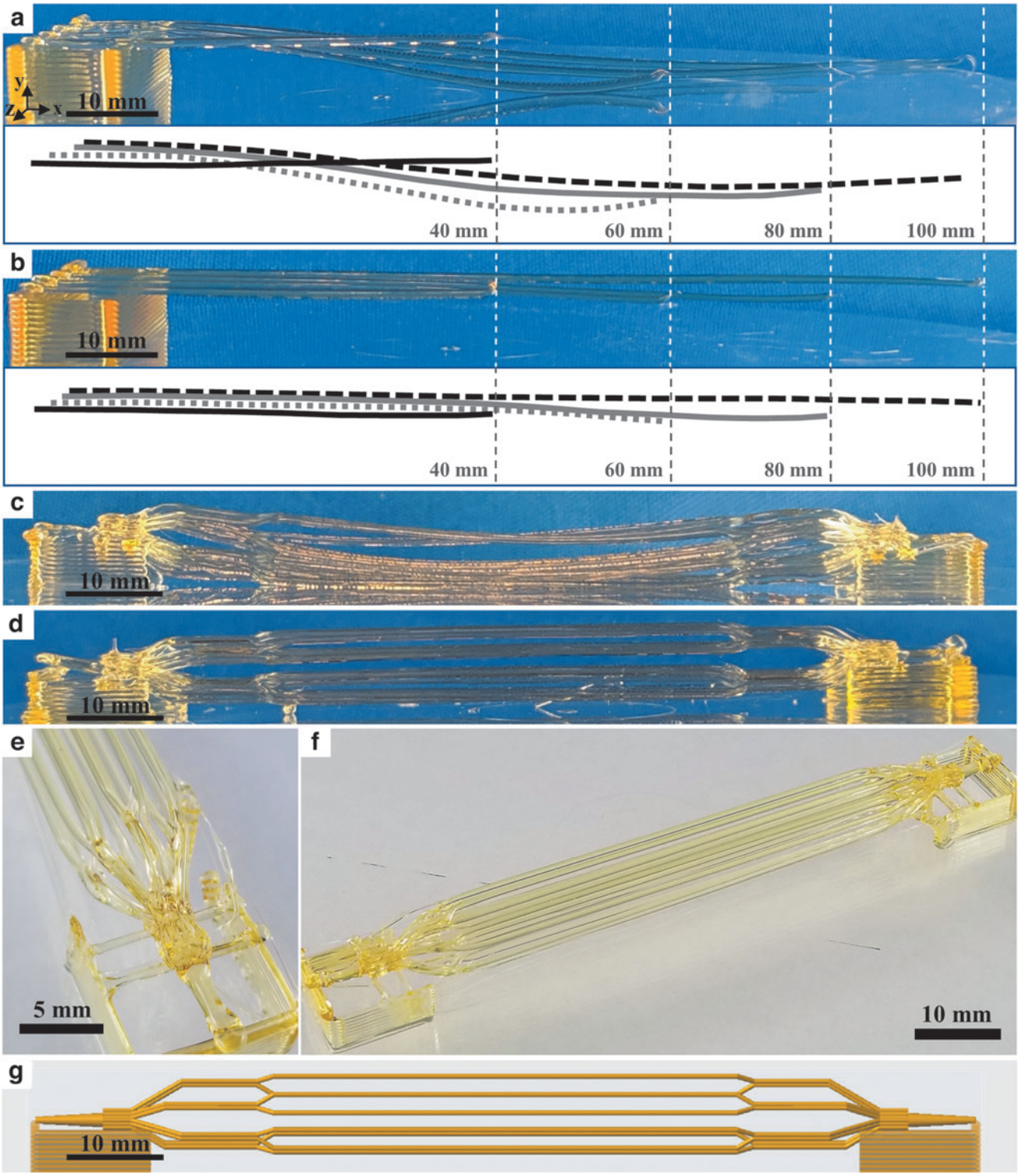

FIG. 5. Maximum cantilever filament length of sugar glass variations and printing of branched networks. Samples are: **(a)** original sugar glass ink with digital filament trace and **(b)** sucrose-only (S100) sugar glass ink with digital filament trace. Filament lengths of 40 mm (*solid black line*), 60 mm (*dotted gray line*), 80 mm (*solid gray line*), and 100 mm (*dashed black line*) were printed (from *front to back*). The nozzle of the printer head was set to 80°C to print the original ink and to 95°C to print the S100 ink. An 18-branched filamentous network fabricated using **(c)** the original ink (nozzle of the printer head was set to 80°C) and **(d)** the S100 ink (nozzle of the printer head was set to 95°C), both photographed immediately after printing. **(e)** Close-up of the entry way and branch points of the 18-branch construct printed using the S100 ink. **(f)** Angled view of the 18-branch construct printed using the S100 ink. **(g)** The computer-generated drawing used to produce prints shown in panels **(c)** and **(d)**.

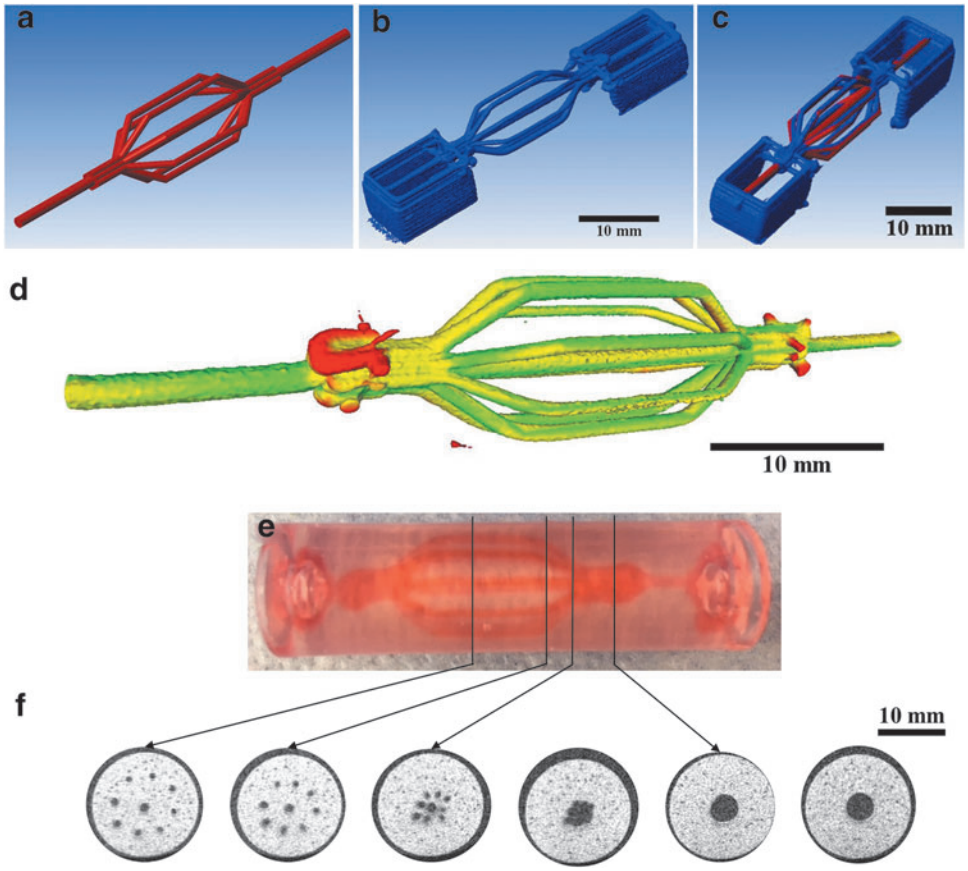

FIG. 6. Assessing the print fidelity of the S100 formulation when printing nine-branch vascular templates and evaluating subsequent perfusable alginate constructs generated using these templates. **(a)** CAD model of the vascular network. **(b)** 3D reconstruction of the 3D-printed vascular template along with supporting structures. **(c)** Isometric view of the CAD model (*red*) superimposed onto the resulting printed vascular template (*blue*). **(d)** Heat map showing minor (*green*, 0–0.25 mm), intermediate (*yellow/orange*, 0.25–0.75 mm), and major (*red*, ≥0.75 mm) deviations of the 3D-printed construct when compared with the CAD model. **(e)** Alginate construct irrigated using a 9-branch vascular template 3D printed using the S100 formulation. **(f)** Shown are μCT images of cross-sections taken at various positions along the perfusable alginate construct shown in **(e)**. For all prints, the S100 formulation was used, and the nozzle of the printer head was set to 95°C. μCT, micro-computed tomography.

encapsulated cells. Encapsulated MIN6 cell viability was assessed around channels formed from original and S100 sugar glass templates. As shown in Figure 7, no significant acute cytotoxic effects were observed with S100 sugar glass templates when compared with alginate-only casts. A small but significant reduction in MIN6 viability was noted with the original formulation when compared with alginate-only casts. From live/dead staining profiles (Fig. 7a, b), it appears that regions closer to the channels created by the original ink exhibit more cell death. Further outward, the viability staining better resembles the condition without any sugar glass, which is shown for comparison in Figure 7c.

Discussion

This work demonstrates the application of a custom printing system and an array of characterization methods to assess and improve the properties of a sacrificial sugar glass ink for use in artificial vascularization strategies. A reliable platform for 3D printing sacrificial vascular templates could streamline the fabrication of perfusable biological systems that would significantly contribute to the advancement of tissue engineering. Namely, this technology could lead to the conception of cm-scale vascularized artificial organs and biomimetic 3D cell culturing devices, as well as facilitate prolonged biological studies. Such advancements depend on the 3D printability of non-conventional materials such as sugar glass.

Referring to the design considerations summarized in Table 1, we optimized a sugar glass formulation (S100) that can be used to print cantilever structures over 10 cm long as well as complex vascular templates with up to 18 branches and over 8 cm in length. Cantilever filaments form the basis for generating single inlet/outlet vascular templates by facilitating the fabrication of branched lattices without the need for supporting structures. The capacity to 3D print longer and more stable cantilevers paves the way for larger, cm-scale constructs and more complex branching.

This work also demonstrates that the 3D geometries of CAD models are consistently conserved when printing with the S100 ink formulation in the x-, y-, and z-axes simultaneously. This ink generates constructs that are stable at room temperature for over a week and can withstand ground shipment times of over 3 h. A summary of all sugar glass formulations evaluated in this work can be found in the Supplementary Material (Supplementary Table S1).

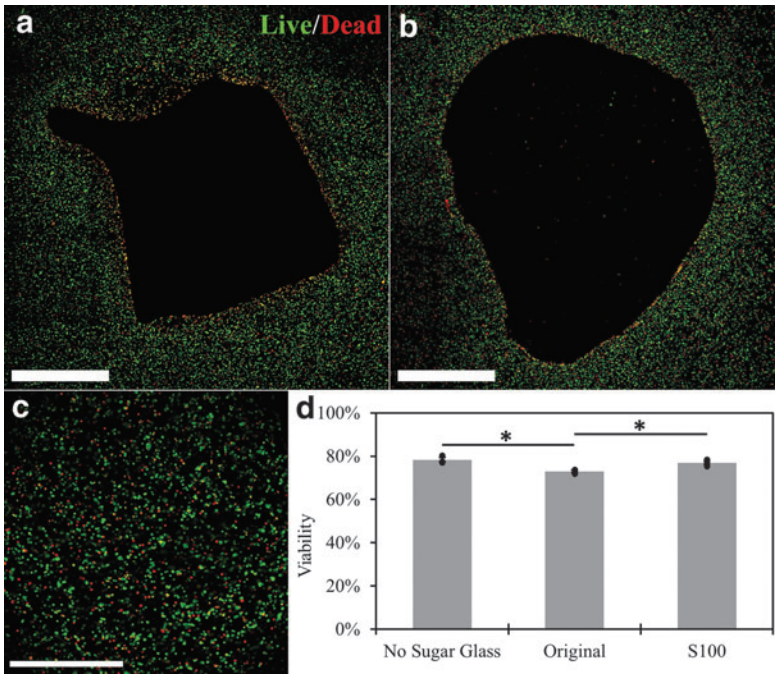

FIG. 7. Viability of MIN6 cells in alginate macroencapsulation devices artificially vascularized using sacrificial sugar glass formulations. Live (*green*, calcein AM) and dead (*red*, ethidium homodimer-1) MIN6 cells around a channel formed using the **(a)** original and **(b)** S100 formulations (2-mm scale bars). **(c)** Live/dead staining of MIN6 cells within an avascular construct (no sugar glass printing performed, 500-μm scale bar). **(d)** Viability quantification of the three conditions based on fluorescence intensity. *$p < 0.05$ by one-way ANOVA and Tukey HSD *post hoc* test. $p < 0.05$ for difference >5% between S100 and control by two one-sided tests, indicating practical equivalency.

Our findings indicate that sugar glass materials with high T_g present distinct advantages when 3D printing self-supporting lattices. We demonstrated that materials with T_g exceeding room temperature resulted in improved printability and more stable constructs. In this work, printability is considered in the context of generating vascular templates and is associated with the capacity to print mechanically stable and multi-branched networks without supporting materials. For our envisioned application of engineering a bioartificial pancreas, the ability of printing cm-scale self-supporting sacrificial networks is also of importance.

By increasing the sucrose content of the ink formulations and adding dextran, an increase in T_g was observed—consistent with blending relationships such as the Gordon-Taylor equation and Couchman-Karasz model.[36,37] A high T_g encourages rapid solidification, rendering the printed filaments strong enough to withstand the dynamic forces associated with 3D printing and specifically those exerted by this printer's cooling air jets. This was demonstrated through improved ink printability and construct stability in the S100 formulation, generating networks that may be suitable for scaled-up tissue engineering applications.

Of note, complex geometries such as the 9-branch structure in Figure 6a–d were not possible with the original formulation due to the rapid onset of significant creeping deformations, particularly at the entryways and for cm-scale constructs envisioned in bioartificial pancreas applications (Fig. 5c–e). Moreover, due to the reduced resistance to bending, constructs printed with the original ink were difficult to manipulate without deforming them—particularly larger, more complex prints. Further optimizations of the platform may be performed to improve smoothness at the printed branch junctions, which would facilitate stable flow during the perfusion of irrigated tissue constructs. In addition to improved printability, the T_d (Fig. 1a, b) and dissolution kinetics (Fig. 2) of the sucrose formulations remained largely unchanged.

A similar T_d indicates a comparable upper limit in 3D printing temperature settings, whereas the conserved dissolution kinetics suggest that the evacuation efficiency of the new formulations would be similar to that of the original material. Efficient removal of the sacrificial material is important in maintaining artificial tissue viability and streamlining the biofabrication process.

To compare printed constructs between formulations, the viscosities at which the inks were printed were set to be equal. Temperature-dependent viscosity models were used to predict the viscosity of the ink formulations and set the nozzle temperature of the printer head. Notably, the printer head has dual temperature control functionality on both the nozzle and syringe barrel. Although barrel and nozzle temperatures could potentially be optimized, effects of temperature on printability and print quality were not observed within the ranges used (data not shown).

A notable observation with the inks presented in this work is the higher degree of caramelization compared with the materials prepared by other groups.[13,31] This is a result of heating the material to 175°C and caramelizing the sugar. It has been demonstrated that the T_g of sugar glass is influenced by caramelization, specifically through heating conditions[33,40] In the case of the original and S100 ink preparation processes, the final heating temperature, holding time, and estimated average heating rate would be considered low.

As such, our preparation method would be characterized by the degradation of sugar into smaller molecules and, thus, a decreased T_g when compared with the starting materials.[33,40] This is a possible explanation for why the T_g of the S100 formulation (40.0 ± 0.9°C, Fig. 1a) was measured to be less than that of pure sucrose (60°C). A relatively low level of caramelization is supported by our spectroscopic analysis of the degree of caramelization (Fig. 1e, f). The S100 formulation was found to have a low concentration of HMF, a commonly used intermediate of the Maillard reaction to measure caramelization, and a lower absorbance at 420 nm when compared with the original ink.

These results suggest that the S100 formulation was subjected to a lower degree of caramelization. Here, we characterized the degree of caramelization using only spectroscopy.

The caramelization of our materials also highlights the limitations of our platform. We observed browning of the ink after prolonged periods (>80 h) of being held within the printer head. This indicates thermal instability when held at high temperatures and therefore limitations regarding long printing times and heated storage of this material. In addition, due to the caramelization of the ink, the use of photopolymerization to solidify a cell-laden matrix around the printed network would result in shadowing artefacts. The incorporation of sugar alcohols could potentially be used to further develop this ink and make it more optically transparent. Sugar alcohols have been used to fabricate rigid 3D-printed filaments and are more resistant to browning than sugars.[30,31]

In addition to caramelization, water content can also have a significant influence on the T_g of sugar glasses by imparting a plasticization effect.[39] Generally, a higher water content has been associated with a decrease in T_g. It has been reported that the water content of sugar glasses derived from sucrose and glucose is directly related to the temperature to which the sugar is heated.[41] Of note, molten sugar heated to 145–154°C (also referred to as ''hard crack'' in food science) has been reported to contain 1–3% water.[41–43] In preparing all the materials presented in this article, all formulations were heated to a final temperature of 175°C. Therefore, the sugar glasses presented here likely contain minimal water.

Moreover, only decreases in mass of <1% were measured at 125°C in our thermogravimetric analyses for the original, S100, and S100D1 formulations, alluding to similar water content across the formulations. Exposure to ambient moisture post-printing is also important to consider when storing 3D prints. Although current sugar constructs are stored in controlled, dry environments, we have shown that constructs printed with the S100 formulation can be stored and shipped in ambient conditions for up to 16 days (Fig. 4).[31]

The sole use of sucrose in the S100 formulation was expected to result in crystallization due to supersaturation.[42] Although other groups have used additions of glucose and fructose to circumvent this, no crystallization in this work was qualitatively observed and no crystallization events in our differential scanning calorimetry analysis were detected. We hypothesize that crystallization was prevented by first heating the mixture to 90°C and completely dissolving all sugar crystals before proceeding to the final heating stage. In addition, the use of RO water (i.e., minimal particles) could have prevented the nucleation of sucrose crystals and thus avoided crystallization. As discussed earlier, the sucrose solution was also subjected to the early stages of caramelization and slow heating rates.

This type of thermal treatment promotes the degradation of sucrose into smaller molecules such as glucose and fructose, which could further discourage crystallization.[40] It has also been reported that nucleation in sucrose solutions can be reduced through rapid agitation and active boiling, which are two characteristics present in our described heating process.[43] To explore this further in sugar glass inks such as the S100, future work could include studying crystallization dynamics using time-lapse microscopy.[44,45]

Dextran was added to the carbohydrate material to further increase T_g and improve the optical transparency of the ink. The addition of dextran, along with the other carbohydrates, before the heating process resulted in inks with lower T_g when compared with their dextran-free counterparts (data not shown). The presence of dextran during the heating process resulted in a noticeably more viscous solution throughout the heating process, and it is postulated that this change in rheological properties inhibited heat transfer and water evaporation.

This hypothesis is based on the assumptions that the active boiling and stirring are the dominant modes of heat transfer and that the increase in viscosity significantly slowed down liquid flow within the beaker. This phenomenon can be explored by additional rheological characterizations of the dextran formulations as well as heat and mass transport computational modeling. This alteration in transport dynamics is hypothesized to have increased the water content of the final sugar glass and affected the degree of caramelization, either of which could have led to the lower T_g values.

Consequently, dry dextran was added to the molten carbohydrate solution only after completing the heating process. Although this modification increased T_g Figure 1a, the resulting formulations were associated with extrusion and consistency challenges (Supplementary Table S1).

The flexural strength and resistance to bending are important characteristics when considering the fabrication, manipulation, transport, storage, and use (i.e., pouring cell-laden hydrogel precursor over the printed constructs) of 3D-printed carbohydrate networks. Although the mechanical strength of both the original and sucrose (S100) inks were found to be similar, these measurements were highly variable. This could be the result of the amorphous nature of the material, as well as the varying conditions throughout the transport, preparation, and storage of the test samples. The S100 ink was found to exhibit a greater flexural modulus than the original formulation (Fig. 3), indicating an improved resistance to bending.

This result could suggest that an increase in T_g may generate more robust structures and vascular molds. Both the original and S100 inks demonstrated greater strength and flexural modulus values than the material presented by Miller *et al.*, which was characterized with a maximum load of 28 MPa and a Young's modulus of 1 GPa.[13] Notably, the comparison of our material's flexural modulus and Miller's Young's modulus assumes an isotropic property of the sugar glasses.

This increase is believed to be the result of a higher degree of caramelization and decreased water content compared with the sugar glass formulation reported by Miller *et al.*, which employed a lower maximum heating temperature (165°C).[13]

The greater flexural modulus observed with S100 is also consistent with what we observed in Figure 5a and b when evaluating the capacity of the inks to generate cantilever structures. Although it may be possible to determine whether the measured flexural modulus corresponds to the recorded

maximum cantilever length, we suspect that creep, in addition to static forces, would influence the deflection of these structures. While studying the filaments over time (Fig. 4), we measured a deflection of $2.2 \pm 0.3\%$ for the original formulation within the first hour after printing. Moreover, forces associated with printing (e.g., pulling forces and drag from the cooling air jets) could also influence the deformation of filaments during printing.

Although sugar glasses could be stored within controlled environments under vacuum, the capacity to store 3D-printed sacrificial templates in ambient conditions would improve the accessibility of this biofabrication approach. The ambient stability of suspended filaments printed from sugar glass was improved by generating an ink from only sucrose (Fig. 4). This is hypothesized to have occurred because of improvements in thermal stability (i.e., a higher T_g) and mechanical rigidity (i.e., increased flexural modulus).

Despite the S100 ink demonstrating a higher degree of print fidelity when generating sugar glass networks (Figs. 5 and 6), once the 3D-printed constructs were used to irrigate alginate devices, the resulting channels differed slightly in diameter and in wall smoothness (Figs. 6 and 7). In our system, calcium chloride is used to accelerate alginate gelation around the sacrificial vascular templates. However, carbohydrate glass dissolution and alginate internal gelation still occur concurrently.[21] Moreover, alginate swelling is expected to occur due to osmotic pressure changes caused by both the gelation and the subsequent water incubation steps before μCT—further explaining the deviations observed.

To minimize the effects of concurrent carbohydrate glass dissolution and alginate gelation/swelling, constructs 3D printed using the S100 formation can be coated with biocompatible polymers such as poly(D-lactide-co-glycolide), as done by the Miller group.[11]

Here, the smallest channel size presented is 1 mm in diameter. Although smaller-diameter filaments can be generated using carbohydrate inks ($\sim$0.4 mm lower limit for original ink),[14] the resulting channels would be more prone to limitations in channel patency and increased pressure drops across devices. In the context of generating intravascular implants, small channel sizes also increase the risk of thrombosis.[46] To control the diameter of printed filaments, a governing equation (Eq. [2]) can be derived from a mass balance around the printing nozzle.[14,25,47]

$$D = A \cdot \sqrt{\frac{v_e}{v_p}} \tag{2}$$

where D is the printed filament diameter, A is a constant that accounts for the printing nozzle inner diameter, v_e is the extrusion speed, and v_p is the printing or nozzle translational speed. The original formulation has been shown to closely follow this relationship in our previous publication, and the S100 ink behaved similarly when studied in this work (data not shown).[14]

Finally, this work supports that the S100 ink has minimal cytotoxic effects toward MIN6 cells encapsulated in alginate. MIN6 cells were selected for these experiments due to their sensitivity to glucose, particularly high oxygen consumption rate, and widespread use in developing bioartificial pancreatic tissue.[48–50] Under similar conditions, the original formulation was found to have decreased the cell viability, which could be a result of the high proportion of glucose used to prepare the ink. Beta cells such as the MIN6 cell line sense glucose levels through transport channels that are active even in the absence of insulin.

As such, this cell type can be subject to higher sensitivity to glucose toxicity via oxidative stress pathways.[51] The different ink formulations may also differ in the degree of polymerization, which could affect local osmolarity during ink dissolution. In addition to cell viability, future work should also examine cell function (e.g., insulin secretion in beta cells) after exposure to sugar glass to identify any possible adverse effects in live cells.

The optimized sucrose ink in this work has demonstrated distinct advantages when considering inks developed by other groups. Of note is the ability to print vertical filaments and long cantilever structures (Fig. 5a, b). The S100 ink has demonstrated a high degree of printability and stability when compared with the original ink used in our previous work published in 2017.[14] The preparation steps of this ink are relatively simple and require only a hotplate stirrer with feedback temperature control, whereas other carbohydrate inks can require vacuum and longer preparation times.[31]

Nevertheless, it is important to note that a different sugar formulation may ultimately be more appropriate depending on the specific tissue engineering application of interest. For instance, the results presented in this work may be most generalizable for others who use similar printing platforms and aim at generating parallel geometries (i.e., cm-scale branched networks with $\sim$1-mm channel diameters). Table 2 provides the context for which 3D-printed sugar glass has been implemented in the field thus far by summarizing the corresponding processing factors and material properties.

The work presented in this article provides a comprehensive approach in engineering 3D-printed sacrificial materials, which includes thermophysical, mechanical, cytocompatible, and logistics characterization. This provides a strong foundation for investigating other candidate sacrificial inks. Future studies using our custom printing system and characterization approach would aim at filling gaps within the field and possibly extending this to investigating non-sugar-based sacrificial materials as well.

Conclusion

This work demonstrates an improvement of the 3D printing system first developed by Miller *et al.* and Bellan *et al.* and advanced by Bégin-Drolet *et al.* through a material optimization approach.[13,14,23] By increasing the T_g of a previously published ink, a higher degree of stability and printability in the sugar glass ink was achieved. Rheological analysis of these materials demonstrates that the temperature-viscosity relationship of sugar glass inks can be well characterized by the Williams-Landel-Ferry equation. Our experiments show that the dissolution kinetics and T_d are largely unaffected by an increase in sucrose content and the addition of small quantities of dextran.

Within the studied ink formulations, an increase in T_g was associated with an increase in flexural modulus and improved printability. Meanwhile, the effect of the material formulation on the flexural strength was not found to be significant. The viability of MIN6 cells encapsulated in alginate and cast around the S100 formulation was not significantly affected by the new formulation.

Table 2. Overview of Current Extrusion-Based Sacrificial Sugar Glass Inks for the Fabrication of Perfusable Devices

	Printing parameters				*Material properties*								*Perfusable construct characteristics*		
Ink	*Printer features*	*Printing temperature (°C)*	*Nozzle diameters (mm)*	*Filament diameters (μm) (v_p)*	T_g *(°C)*	T_d *(°C)*	*Viscosity (Pa·s)*[a]	*Max. Strength (MPa)*	*Modulus (GPa)*	*Optical Properties*	*Cell types Used*	*Storage Conditions*	*Capacity for 3D Branching*	*Perfusable Construct Materials*	*Source*
Sucrose	Barrel and nozzle heater with piston plunger and forced air cooling at nozzle	Nozzle: 95; Barrel: 110	1.0	0.4–3.1 mm (4–140 mm/min)	40.0	186.2	529 (0.5 s^{-1})	68.0	10.46 (Flexural)	A_{420} = 0.154 (150 mg/mL)	MIN6	In desiccated container or at ambient conditions	Yes	Alginate	This work
Sucrose-glucose	Barrel and nozzle heater with piston plunger and forced air cooling at nozzle	Nozzle: 80; Barrel: 110	1.0	0.4–3.1 mm (4–140 mm/min)	26.2	172.6	529 (0.5 s^{-1})	80.0	6.47 (Flexural)	A_{420} = 0.432 (150 mg/mL)	NR	In desiccated container	Yes	PDMS	This work,[14]
Sucrose-glucose	Barrel heater with air pressure dispenser and cooling fan	Barrel: 90	0.15	200–1000 (25–250 mm/min)	NR	NR	150 (1 s^{-1})	NR	NR	NR	NR	Closed box with silica beads and low humidity	Yes	PDMS	[28]
Sucrose-glucose-dextran	Barrel heater with air pressure dispenser and cooling fan	Barrel: 90	0.15	120–350 (20–180 mm/min)	NR	NR	1100 (1 s^{-1})	NR	NR	NR	NR	Closed box with silica beads and low humidity	Yes	PDMS	[28]
Sucrose-glucose-dextran	Barrel heater with air pressure dispenser	Barrel: 110	0.84, 1.2	150–1100 (1–3000 mm/min)	NR	NR	NR	28	1 (Young's)	Transmits light wavelengths 365–550 nm	HUVEC, 10T1/2, HEK, primary rat hepatocytes, rat implants	Under vacuum at 45°C	Only 2D prints	Agarose, alginate, PEG, fibrin, and Matrigel	[13]
Isomalt	Barrel heater with piston plunger (100–200 psi) and pressure transducer	Barrel: 130	0.11	50–800 (1–0.007 mm/s)	NR	NR	3 (empirically determined zero-shear)	NR	2.6 (Flexural)	NR, but visually clear	NR	In mineral oil or in a dry box	Not shown but likely capable	Epoxy resin and agarose	[31,32]
Maltitol	Barrel heater with air pressure dispenser (2–3 bar)	Barrel: 150	0.3	25–1400 (4600–300 mm/min)	NR	NR	NR	NR	NR	NR but visually clear	SKOV3	NR	Only 2D prints	PDMS	[30]
Glucose-fructose	Barrel heater	Barrel: 100	0.03	NR	NR	NR	NR	NR	NR	NR but visually yellowish brown	NR	NR	Only 2D prints	PDMS	[24]

[a]Values in parenthesis indicate shear rate used in the corresponding rheometry experiments.

HEK, human embryonic kidney cells; HUVEC, human umbilical vein endothelial cells; MIN6, mouse insulinoma 6; NR, information that was not reported; PDMS, polydimethylsiloxane; PEG, polyethylene glycol.

The results suggest that rigorous material characterization and optimization can improve the outlook of sugar printing in tissue engineering applications, offering improved thermophysical stability, demonstrated printability, and simple preparation of artificial vascular templates. The design considerations and characterization methods described in this work may be expanded and applied to a variety of candidate sacrificial ink materials with the long-term goal of increasing the relevance of sacrificial molding in artificial tissue construction.

In addition to advancements in vascularized tissue fabrication, improving the capacity to 3D print sugar glass could have implications in other avenues such as culinary or food engineering applications. Shedding light on strategies for optimizing non-conventional 3D printing methods also contributes to the overall understanding of 3D printing and promotes the development of other non-conventional inks and additive manufacturing platforms.

Acknowledgments

The authors would like to thank Petr Fiurasek for his guidance, as well as Marc-André Dussault, Jean-François Provost-Blais, and Patrice Roberge (Université Laval) for their 3D printing instruction and support in preparing figures for this article. They would also like to recognize the work of Philippe Legros (Université Laval) for his contribution to μCT imaging.

Authors' Contributions

B.N.M. contributed to the conceptualization, methodology, validation, formal analysis, investigation, data curation, writing, editing, visualization, supervision, and project administration. S.A.F. contributed to the conceptualization, methodology, editing, visualization, supervision, and project administration. S.C. contributed to the software, validation, formal analysis, investigation, data curation, writing, editing, and visualization. G.G.R. contributed to the methodology, validation, formal analysis, investigation, writing, editing, and visualization. M.A.F. and T.L. contributed to the methodology, validation, formal analysis, investigation, resources, data curation, writing, editing, visualization, supervision, and funding acquisition. J.R. contributed to the resources, editing, supervision, and funding acquisition. A.B.D. contributed to the software, resources, editing, supervision, and funding acquisition. R.L.L. contributed to the methodology, validation, formal analysis, resources, editing, supervision, and funding acquisition. C.A.H. contributed to the conceptualization, methodology, formal analysis, resources, editing, supervision, project administration, and funding acquisition.

Author Disclosure Statement

No competing financial interests exist.

Funding Information

This research was undertaken thanks to funding from the Canada Research Chairs program, 950-231290, the Juvenile Diabetes Research Foundation (JDRF), 1-PNF-2016-249-S-B, Diabetes Québec, the Quebec Cell, Tissue and Gene Therapy Network—ThéCell (a thematic network supported by the Fonds de recherche du Québec–Santé) and the Canadian Foundation for Innovation (CFI), 35507. Several research networks supported this project through travel awards and networking opportunities, including ThéCell, the McGill Regenerative Medicine Network (MRM), the Cardiometabolic Health, Diabetes and Obesity (CMDO) Research Network, the Quebec Centre for Advanced Materials (QCAM), the Montreal Diabetes Research Center (MDRC), and the PROTEO Network. B.N.M. received scholarships from Diabetes Québec, the Natural Sciences and Engineering Research Council (NSERC) of Canada, the Fonds de recherche du Québec—Nature et technologies (FRQNT), and the Summer Undergraduate Research in Engineering (SURE) program at McGill University.

Supplementary Material

Supplementary Figure S1
Supplementary Figure S2
Supplementary Table S1
Supplementary Video S1
Supplementary Video S2

References

1. Naganuma H, Nishinakamura R. From organoids to transplantable artificial kidneys. Transpl Int 2019;32:563–570.
2. Moeun BN, Da Ling S, Gasparrini M, et al. Islet encapsulation: A long-term treatment for type 1 diabetes. In: Caplan M, eds. Reference Module in Biomedical Sciences. Amsterdam, Netherlands: Elsevier, 2019.
3. Ohashi K, Yokoyama T, Yamato M, et al. Engineering functional two-and three-dimensional liver systems *in vivo* using hepatic tissue sheets. Nat Med 2007;13:880.
4. Hirt MN, Hansen A, Eschenhagen T. Cardiac tissue engineering: State of the art. Circ Res 2014;114:354–367.
5. Kaully T, Kaufman-Francis K, Lesman A, et al. Vascularization—The conduit to viable engineered tissues. Tissue Eng Part B Rev 2009;15:159–169.
6. Auger FA, Gibot L, Lacroix D. The pivotal role of vascularization in tissue engineering. Ann Rev Biomed Eng 2013;15:177–200.
7. Papas KK, Avgoustiniatos ES, Suszynski TM. Effect of oxygen supply on the size of implantable islet-containing encapsulation devices. Panminerva Med 2016;58:72–77.
8. Dew L, MacNeil S, Chong CK. Vascularization strategies for tissue engineers. Regen Med 2015;10:211–224.
9. Mironov V, Boland T, Trusk T, et al. Organ printing: Computer-aided jet-based 3D tissue engineering. Trends Biotechnol 2003;21:157–161.
10. Rouwkema J, Rivron NC, van Blitterswijk CA. Vascularization in tissue engineering. Trends Biotechnol 2008;26:434–441.
11. Jain RK, Au P, Tam J, et al. Engineering vascularized tissue. Nat Biotechnol 2005;23:821.
12. Skylar-Scott MA, Uzel SG, Nam LL, et al. Biomanufacturing of organ-specific tissues with high cellular density and embedded vascular channels. Sci Adv 2019;5:eaaw2459.
13. Miller JS, Stevens KR, Yang MT, et al. Rapid casting of patterned vascular networks for perfusable engineered three-dimensional tissues. Nat Mater 2012;11:768.
14. Bégin-Drolet A, Dussault M-A, Fernandez SA, et al. Design of a 3D printer head for additive manufacturing of sugar glass for tissue engineering applications. Addit Manuf 2017;15:29–39.
15. Kolesky DB, Homan KA, Skylar-Scott MA, et al. Three-dimensional bioprinting of thick vascularized tissues. Proc Natl Acad Sci 2016;113:3179–3184.

16. Kolesky DB, Truby RL, Gladman AS, et al. 3D bioprinting of vascularized, heterogeneous cell-laden tissue constructs. Adv Mater 2014;26:3124–3130.
17. Galván NTN, Paulsen SJ, Kinstlinger IS, et al. Blood flow within bioengineered 3D printed vascular constructs using the porcine model. Front Cardiovasc Med 2021;8:479.
18. Yang K, O'Cearbhaill ED, Liu SS, et al. A therapeutic convection–enhanced macroencapsulation device for enhancing β cell viability and insulin secretion. Proc Natl Acad Sci 2021;118:e2101258118.
19. Wu W, DeConinck A, Lewis JA. Omnidirectional printing of 3D microvascular networks. Adv Mater 2011;23:H178–H183.
20. Toohey KS, Sottos NR, Lewis JA, et al. Self-healing materials with microvascular networks. Nat Mater 2007;6:581.
21. Therriault D, White SR, Lewis JA. Chaotic mixing in three-dimensional microvascular networks fabricated by direct-write assembly. Nat Mater 2003;2:265–271.
22. Kinstlinger IS, Saxton SH, Calderon GA, et al. Generation of model tissues with dendritic vascular networks via sacrificial laser-sintered carbohydrate templates. Nat Biomed Eng 2020:1–17.
23. Bellan LM, Singh SP, Henderson PW, et al. Fabrication of an artificial 3-dimensional vascular network using sacrificial sugar structures. Soft Matter 2009;5:1354–1357.
24. Koyata Y, Ikeuchi M, Ikuta K. Sealless 3-D microfluidic channel fabrication by sacrificial caramel template direct-patterning. In: 2013 IEEE 26th International Conference on Micro Electro Mechanical Systems (MEMS) 2013, pp.311–314. IEEE.
25. Miller JS, Stevens KR, Yang MT, et al. Rapid casting of patterned vascular networks for perfusable engineered three-dimensional tissues. Nat Mater 2012;11:768–774.
26. Gauvin-Rossignol G, Legros P, Ruel J, et al. Sugar glass fugitive ink loaded with calcium chloride for the rapid casting of alginate scaffold designs. Heliyon 2018;4:e00680.
27. Farzin A, Miri AK, Sharifi F, et al. 3D-printed sugar-based stents facilitating vascular anastomosis. Adv Healthcare Mater 2018;7:1800702.
28. Pollet AM, Homburg EF, Cardinaels R, et al. 3D sugar printing of networks mimicking the vasculature. Micromachines 2020;11:43.
29. Sooppan R, Paulsen SJ, Han J, et al. *In vivo* anastomosis and perfusion of a three-dimensionally-printed construct containing microchannel networks. Tissue Eng Part C Methods 2016;22:1–7.
30. He Y, Qiu J, Fu J, et al. Printing 3D microfluidic chips with a 3D sugar printer. Microfluid Nanofluid 2015;19:447–456.
31. Gelber M, Hurst G, Comi T, et al. Model-guided design and characterization of a high-precision 3D printing process for carbohydrate glass. Addit Manuf 2018;22:38–50.
32. Gelber MK, Bhargava R. Monolithic multilayer microfluidics via sacrificial molding of 3D-printed isomalt. Lab Chip 2015;15:1736–1741.
33. Jiang B, Liu Y, Bhandari B, et al. Impact of caramelization on the glass transition temperature of several caramelized sugars. Part I: Chemical analyses. J Agric Food Chem 2008;56:5138–5147.
34. Van Krevelen DW, Te Nijenhuis K. Properties of Polymers: Their Correlation with Chemical Structure; Their Numerical Estimation and Prediction from Additive Group Contributions. Amsterdam, Boston: Elsevier, 2009.
35. Bond EB, Chhabra R, Isele OEA, et al. Fibers, nonwovens and articles containing nanofibers produced from high glass transition temperature polymers. Google Patents, 2009.
36. Gordon M, Taylor JS. Ideal copolymers and the second-order transitions of synthetic rubbers. I. Non-crystalline copolymers. J Chem Technol Biotechnol 1952;2:493–500.
37. Couchman P. Thermodynamics and the compositional variation of glass transition temperatures. Macromolecules 1987;20:1712–1717.
38. Simperler A, Kornherr A, Chopra R, et al. Glass transition temperature of glucose, sucrose, and trehalose: An experimental and in silico study. J Phys Chem B 2006;110:19678–19684.
39. Icoz DZ, Moraru CI, Kokini JL. Polymer–polymer interactions in dextran systems using thermal analysis. Carbohydr Polym 2005;62:120–129.
40. Vanhal I, Blond G. Impact of melting conditions of sucrose on its glass transition temperature. J Agric Food Chem 1999;47:4285–4290.
41. Hartel RW, Hartel A. Soft Ball to Hard Crack. Candy Bites. Springer, 2014; pp. 29–32. https://link.springer.com/chapter/10.1007/978-1-4614-9383-9_8 Accessed April 14, 2022.
42. Reinheimer MA, Mussati S, Scenna NJ. Influence of product composition and operating conditions on the unsteady behavior of hard candy cooling process. J Food Eng 2010;101:409–416.
43. Van Hook A, Bruno AJ. Nucleation and growth in sucrose solutions. Discuss Faraday Soc 1949;5:112–117.
44. Mazzobre MaF, Aguilera JM, Buera MaP. Microscopy and calorimetry as complementary techniques to analyze sugar crystallization from amorphous systems. Carbohydr Res 2003;338:541–548.
45. Velazquez-Camilo O, Bolaños-Reynoso E, Rodriguez E, et al. Characterization of cane sugar crystallization using image fractal analysis. J Food Eng 2010;100:77–84.
46. Chesnutt JK, Han H-C. Tortuosity triggers platelet activation and thrombus formation in microvessels. J Biomech Eng 2011;133:121004.
47. Heiber J, Clemens F, Graule T, et al. Thermoplastic extrusion to highly-loaded thin green fibres containing Pb (Zr, Ti) O3. Adv Eng Mater 2005;7:404–408.
48. Sato Y, Endo H, Okuyama H, et al. Cellular hypoxia of pancreatic β-cells due to high levels of oxygen consumption for insulin secretion *in vitro*. J Biol Chem 2011;286:12524–12532.
49. Hu S, Martinez-Garcia FD, Moeun BN, et al. An immune regulatory 3D-printed alginate-pectin construct for immunoisolation of insulin producing β-cells. Mater Sci Eng C 2021;123:112009.
50. Fernandez SA, Danielczak L, Gauvin-Rossignol G, et al. An *in vitro* perfused macroencapsulation device to study hemocompatibility and survival of islet-like cell clusters. Front Bioeng Biotechnol 2021;9.
51. Ge Q, Dong Y, Su Q. Effects of glucose and advanced glycation end products on oxidative stress in MIN6 cells. Cell Mol Biol 2010;56:1231–1238.

Address correspondence to:
Corinne A. Hoesli
Department of Chemical Engineering
McGill University
Room 4300, Wong Building, 3610 University Street
Montreal H3A 0C5
Canada

E-mail: corinne.hoesli@mcgill.ca